Chapter 7

Nonlinear Optical Phenomena in Smectic A Liquid Crystals

Boris I. Lembrikov, David Ianetz and Yossef Ben Ezra

Additional information is available at the end of the chapter

http://dx.doi.org/10.5772/intechopen.70997

Abstract

Liquid crystals (LC) are the materials characterized by extremely high optical nonlinearity. Their physical properties such as temperature, molecular orientation, density, and electronic structure can be easily perturbed by an applied optical field. In particular, in smectic A LC (SALC), there is a specific mechanism of the cubic optical nonlinearity determined by the smectic layer normal displacement. The physical processes related to this mechanism are characterized by a comparatively large cubic susceptibility, short time response, strong dependence on the optical wave polarization and propagation direction, resonant spectral form, low scattering losses as compared to other LC phases, and weak temperature dependence in the region far from the phase transition. We investigated theoretically the nonlinear optical phenomena caused by this type of the cubic nonlinearity in SALC. It has been shown that the light self-focusing, self-trapping, Brillouin-like stimulated light scattering (SLS), and four-wave mixing (FWM) related to the smectic layer normal displacement are strongly manifested in SALC. We obtained the exact analytical solutions in some cases and made the numerical evaluations of the basic parameters such as the optical beam width and SLS gain.

Keywords: smectic liquid crystals, second sound, nonlinear optics, cubic nonlinearity, stimulated scattering of light, four-wave mixing, surface plasmon polariton

1. Introduction

Liquid crystals (LC) are characterized by the physical properties intermediate between ordinary isotropic fluids and solids [1]. LC flow like liquids but also exhibit some properties of crystals [1, 2]. The various phases in which such materials can exist are called mesophases [1, 2]. The LC molecules are large, anisotropic, and complex [2]. Dielectric constants, elastic constants, viscosities,

absorption spectra, transition temperatures, anisotropies, and optical nonlinearities of LC are determined by the structure of these molecules [1, 2]. There exist three different types of LC: lyotropic, polymeric, and thermotropic [1, 2]. Lyotropic LC are obtained when an appropriate concentration of a material is dissolved in a solvent [2]. They can demonstrate a one-, two-, or three-dimensional positional order [2]. Liquid crystalline polymers are built up by the joining together the rigid mesogenic monomers [2]. Thermotropic LC exhibit different mesophases depending on temperature [1, 2]. Typically, they consist of organic molecules elongated in one direction and represented as rigid rods [2]. There are two types of LC sample orientation with respect to the boundary: (i) a homeotropic orientation when the long molecular axes are perpendicular to the boundary and (ii) a planar orientation when the long molecular axes are parallel to the boundary [1].

In this work, we consider only thermotropic LC, which are divided into three groups according to their symmetry: nematic LC (NLC), cholesteric LC (CLC), and smectic LC (SLC) [1, 2]. NLC are characterized by some long-range order in the direction of the molecular long axes, while the centers of gravity of the molecules do not have any long range order [1, 2]. The general direction of the molecules is defined by a unit vector function $\vec{n}\ (x,y,z,t)$; $\left|\vec{n}\ (x,y,z,t)\right| = 1$ called director [1, 2]. NLC molecules are centrosymmetric such that the $\vec{n}$ and $-\vec{n}$ directions are equivalent; NLC are optically uniaxial media with a comparatively large birefringence of about 0.2 [1, 2]. LC consisting of chiral molecules yield CLC phase with the helical structure [1, 2]. The molecule centers of gravity in CLC do not have a long range order like in NLC, while the direction of the molecular orientation rotates in space about the helical axis Z with a period of about 300 nm [1, 2]. The smectic LC (SLC) are characterized by the positional long range order in the direction of the elongated molecular axis and exhibit a layer structure [1, 2]. The layer thickness $d \approx 2nm$ is approximately equal to the length of the constituent molecule [1, 2]. SLC can be considered as natural nanostructures. Inside a layer the molecules form a two-dimensional liquid [1, 2]. The layers can easily move one along another because the elastic constant $B \approx 10^6 - 10^7 Jm^{-3}$ related to the layer compression is two orders of magnitude less than the elastic constant related to the bulk compression [1]. There exist different phases of SLC: (i) smectic A LC (SALC) where the molecule long axes are perpendicular to the layer plane; (ii) smectic B LC with the in-layer hexagonal ordering of the molecules; (iii) smectic C LC where the molecules are tilted with respect to the layers; (iv) smectic C^* LC consisting of the chiral molecules and possessing the spontaneous polarization; (v) different exotic smectic mesophases [1]. In this work, we consider only SALC. The SALC layered structure can be described by the one-dimensional mass density wave characterized by the complex order parameter. The modulus of this order parameter describes the mass density and its phase is related to smectic layer displacement $u(x,y,z,t)$ along the direction perpendicular to the layer plane [1]. SALC is an optically uniaxial medium [2].

LC are highly nonlinear optical materials due to their complex physical structures, and their temperature, molecular orientation, mass density, electronic structure can be easily perturbed by an external optical field [2–4]. Almost all known nonlinear optical phenomena have been observed in LC in time scale range from picoseconds to hours, involving laser powers from 10^6 Watt to 10^{-9} Watt, in different configurations such as bulk media, optical waveguides, optical resonators and cavities, and spatial light modulators [3]. For instance, a typical LC slab optical

waveguide is a thin film of LC with a thickness of about $1\mu m$ sandwiched between two glass slides of lower refracted index than LC [2]. Stimulated light scattering (SLS), self-phase modulation (SPM), self-focusing, spatial soliton formation, optical wave mixing, harmonic generation, optical phase conjugation, and other nonlinear optical effects in LC have been investigated [3]. NLC is the most useful and widely studied type of LC [2–4]. However, the practical integrated electro-optical applications of NLC are limited by their large losses of about 20 dB/cm and relatively slow responses [2]. The scattering losses in SALC are much lower, and they can be useful in nonlinear optical applications [2]. Recently, the LC applications in plasmonics attracted a wide interest due to the combination of the surface plasmon polaritons (SPP) strong electric fields and the unique electro-optical properties of LC [4].

We investigated theoretically the nonlinear optical phenomena in SALC related to the specific mechanism of the cubic nonlinearity, which is determined by the smectic layer normal displacement $u(x, y, z, t)$ in the electric field of optical waves and SPP [5–13]. This mechanism combining the properties of the orientational and electrostrictive nonlinearities [2] occurs without the mass density change, strongly depends on the optical wave polarization and propagation direction, and has a resonant form of the frequency dependence. It is characterized by a comparatively short response time similar to acousto-optic processes [2, 14].

The theoretical analysis of the nonlinear optical phenomena in SALC related to the layer displacement was based on the simultaneous solution of the Maxwell equations for the optical waves propagating in SALC and the equation of motion for the SALC layers in the electric field of these waves. We used the slowly varying amplitude approximation (SVAA) [14]. We investigated the following nonlinear optical effects in SALC based on the layer displacement nonlinearity: self-focusing and self-trapping, SLS, and four-wave mixing (FWM) [5–10]. We applied the developed theory of the nonlinear optical phenomena in SALC to the SPP interactions in SALC [11–13]. The SPP stimulated scattering in SALC and the metal/insulator/metal (MIM) plasmonic waveguide with the SALC core are theoretically studied [11–13]. The detailed calculations and complicated explicit analytical expressions can be found in Refs [5–13]. In this chapter, we describe the general approach to the theoretical analysis of the nonlinear optical phenomena in SALC and present the main results.

The chapter is constructed as follows. The equation of motion for the smectic layer normal displacement $u(x, y, z, t)$ in the electric field is derived in Section 2. The self-focusing and self-trapping of the optical wave in SALC are considered in Section 3. The SLS in SALC is investigated in Section 4. The FWM in SALC is analyzed in Section 5. The SPP interaction in SALC is discussed in Section 6. The conclusions are presented in Section 7.

2. The smectic layer equation of motion

The structure of the homeotropically oriented SALC in an external electric field $\vec{E}(x, y, z, t)$ is presented in **Figure 1**.

The hydrodynamics of SALC is described by the following system of Eq. [1]

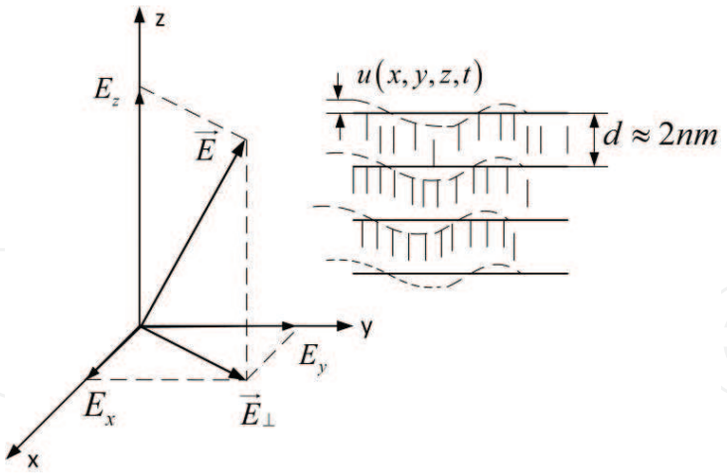

Figure 1. Homeotropically oriented SALC in an external electric field $\vec{E}\ (x, y, z, t)$.

$$\text{div}\ \vec{v} = 0 \tag{1}$$

$$\rho \frac{\partial v_i}{\partial t} = -\frac{\partial \Pi}{\partial x_i} + \Lambda_i + \frac{\partial \sigma'_{ik}}{\partial x_k} \tag{2}$$

$$\Lambda_i = -\frac{\delta F}{\delta u_i} \tag{3}$$

$$\sigma'_{ik} = \alpha_0 \delta_{ik} A_{ll} + \alpha_1 \delta_{iz} A_{zz} + \alpha_4 A_{ik} + \alpha_{56}(\delta_{iz} A_{zk} + \delta_{kz} A_{zi}) + \alpha_7 \delta_{iz} \delta_{kz} A_{ll} \tag{4}$$

$$A_{ik} = \frac{1}{2}\left(\frac{\partial v_i}{\partial x_k} + \frac{\partial v_k}{\partial x_i}\right) \tag{5}$$

$$v_z = \frac{\partial u}{\partial t} \tag{6}$$

Here, $\vec{v}$ is the hydrodynamic velocity, ρ is the mass density, Π is the pressure, $\vec{\Lambda}$ is the generalized force density, σ'_{ik} is the viscous stress tensor, α_i are the viscosity Leslie coefficients, $\delta_{ik} = 1, i = k; \delta_{ik} = 0, i \neq k$, and F is the free energy density of SALC. Typically, SALC is supposed to be incompressible liquid according to Eq. (1) [1]. For this reason, we assume that the pressure $\Pi = 0$ and the SALC-free energy density F do not depend on the bulk compression [1]. The normal layer displacement $u(x, y, z, t)$ by definition has only one component along the Z axis. In such a case, the generalized force density $\vec{\Lambda}$ has only the Z component according to Eq. (3): $\vec{\Lambda} = (0, 0, \Lambda_z)$. Eq. (6) is specific for SALC since it determines the condition of the smectic layer continuity [1]. The SALC free energy density F in the presence of the external electric field $\vec{E}\ (x, y, z, t)$ has the form [1]

$$F = \frac{1}{2}B\left(\frac{\partial u}{\partial z}\right)^2 + \frac{1}{2}K\left(\frac{\partial^2 u}{\partial x^2} + \frac{\partial^2 u}{\partial y^2}\right)^2 - \frac{1}{2}\varepsilon_0 \varepsilon_{ik} E_i E_k \tag{7}$$

where K is the Frank elastic constant associated with the SALC purely orientational energy, ε_0 is the free space permittivity, and ε_{ik} is the SALC permittivity tensor including the nonlinear terms related to the smectic layer strains. It is given by [1]

$$\begin{aligned}\varepsilon_{xx} = \varepsilon_{yy} = \varepsilon_\perp + a_\perp \frac{\partial u}{\partial z}; \varepsilon_{zz} = \varepsilon_\parallel + a_\parallel \frac{\partial u}{\partial z};\\ \varepsilon_{xz} = \varepsilon_{zx} = -\varepsilon_a \frac{\partial u}{\partial x}; \varepsilon_{yz} = \varepsilon_{zy} = -\varepsilon_a \frac{\partial u}{\partial y}; \varepsilon_a = \varepsilon_\parallel - \varepsilon_\perp\end{aligned} \tag{8}$$

Here, $\varepsilon_\perp, \varepsilon_\parallel$ are the diagonal components of the uniaxial SALC permittivity tensor perpendicular and parallel to the optical axis Z, respectively, and $a_\perp \sim 1; a_\parallel \sim 1$ are the phenomenological dimensionless coefficients. For the smectic layer displacement $u(x, y, z, t)$ depending on z, the purely orientational second term in the free energy density F (7) can be neglected. Indeed, for the typical values of B and $K \sim 10^{-11}N$ [1], the following inequality is valid: $Kk_{S\perp}^2 \ll B$ where $k_{S\perp}$ is the in-plane component of the smectic layer displacement wave vector. The contribution of the first term containing the normal layer strain is dominant. We consider the smectic layer normal displacement with $k_{Sz} \neq 0$. Taking into account the assumptions mentioned above and combining Eqs. (1)–(9), we obtain the equation of motion for the smectic layer normal displacement $u(x, y, z, t)$ [5, 6, 10]

$$\begin{aligned}&-\rho\nabla^2 \frac{\partial^2 u}{\partial t^2} + \left[\alpha_1 \nabla_\perp^2 \frac{\partial^2}{\partial z^2} + \frac{1}{2}(\alpha_4 + \alpha_{56})\nabla^2\nabla^2\right]\frac{\partial u}{\partial t} + B\nabla_\perp^2 \frac{\partial^2 u}{\partial z^2}\\ &= \frac{\varepsilon_0}{2}\nabla_\perp^2\left[\frac{\partial}{\partial z}\left(a_\perp\left(E_x^2 + E_y^2\right) + a_\parallel E_z^2\right) - 2\varepsilon_a\left(\frac{\partial}{\partial x}(E_x E_z) + \frac{\partial}{\partial y}\left(E_y E_z\right)\right)\right].\end{aligned} \tag{9}$$

.Here, $\nabla_\perp^2 = \partial^2 u/\partial x^2 + \partial^2 u/\partial y^2$. If the external electric field is absent and the viscosity terms responsible for the decay of the smectic layer displacement are neglected, Eq. (10) coincides with the equation of the so-called second sound (SS) [1]

$$\rho\nabla^2 \frac{\partial^2 u}{\partial t^2} = B\nabla_\perp^2 \frac{\partial^2 u}{\partial z^2}. \tag{10}$$

Generally, for an arbitrary direction of the wave vector $\vec{k}_S$ in SALC, there exist two practically uncoupled acoustic modes: (i) the ordinary longitudinal sound wave caused by the mass density oscillations; (ii) SS wave caused by the smectic layer oscillations [1]. The SS propagation may be considered separately from ordinary sound since B is much less than the elastic constant of the mass density oscillations [1]. The SS dispersion relation corresponding to Eq. (11) has the form [1]

$$\Omega_S = s_0 \frac{k_{S\perp} k_{Sz}}{k_S}; s_0 = \sqrt{\frac{B}{\rho}} \tag{11}$$

Here, $\Omega_S, \vec{k}_S, s_0$ are SS frequency, wave vector and phase velocity, respectively. It is seen from Eq. (11) that SS is neither longitudinal, nor purely transverse, and it vanishes for the wave vectors $\vec{k}_S$ perpendicular or parallel to the layer plane. SS represents the oscillations of the

SALC complex order parameter phase [1]. If we take into account the viscosity terms in Eq. (10), then we can obtain the SS relaxation time τ_S given by

$$\tau_S = 2\rho\left[\alpha_1 \frac{\left(k_{Sx}^2 + k_{Sy}^2\right)k_{Sz}^2}{k_S^2} + \frac{1}{2}(\alpha_4 + \alpha_{56})k_S^2\right]^{-1} \tag{12}$$

SS has been observed experimentally [15–17].

3. Self-focusing and self-trapping of optical beams in SALC

We first consider the self-action effects of the optical waves propagating in an anisotropic inhomogeneous nonlinear medium. The light beam propagation through a nonlinear medium is accompanied by the intensity-dependent phase shift on the wavefront of the beam [2]. Self-focusing of light results from the wavefront distortion inflicted on the beam by itself while propagating in a nonlinear medium [14]. In such a case, the field-induced refractive change Δn has the form $\Delta n = n_2|E|^2$ where $n_2 = const$ [14]. A light beam with a finite cross section also diffracts [14]. At a certain optical power level, the beam self-focusing and diffraction can be balanced in such a way that the beam propagates in the nonlinear medium with a plane wavefront and a constant transverse intensity profile [1]. This phenomenon is called self-trapping of an optical beam [1]. The optical wave propagation in a nonlinear medium is described by the following wave equation for the electric field $\vec{E}\ (x, y, z, t)$ [14]

$$curlcurl\ \vec{E} + \mu_0 \frac{\partial^2 \vec{D}\ L}{\partial t^2} = -\mu_0 \frac{\partial^2 \vec{D}\ NL}{\partial t^2} \tag{13}$$

Here, μ_0 is the free space permeability, $\vec{D}^L$ and $\vec{D}^{NL}$ are the linear and nonlinear parts of the electric induction. In SALC as a uniaxial medium two waves with the same frequency ω can propagate: an ordinary wave with the wave vector $\vec{k}_o$ and an extraordinary one with the wave vector $\vec{k}_e$ [2, 18]. Taking into account the SALC symmetry, we can choose the xz plane as a propagation plane. Then, the ordinary wave is polarized along the Y axis, and its electric field is given by

$$E_{oy} = A_o \exp[i(k_{ox}x + k_{oz}z - \omega t)] + c.c. \tag{14}$$

The extraordinary wave is polarized in the XZ plane having a component along the optical axis Z. The electric field of the extraordinary wave has the form

$$\vec{E}_e = \vec{e}_e A_e \exp[i(k_{ex}x + k_{ez}z - \omega t)] + c.c. \tag{15}$$

Here, $\vec{e}_e = \vec{a}_x e_{ex} + \vec{a}_z e_{ez}$ is the polarization unit vector of the extraordinary wave, $\vec{a}_{x,z}$ are the unit vectors of the X, Z axes, and c.c. stands for complex conjugate. The propagation direction and polarization of the ordinary and extraordinary waves in SALC are shown in **Figure 2**.

http://dx.doi.org/10.5772/intechopen.70997

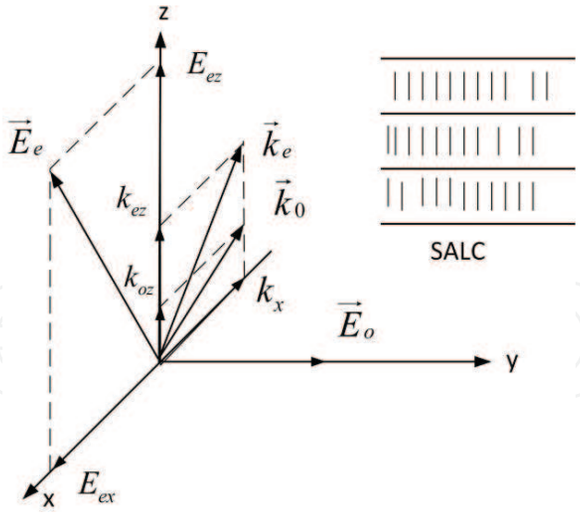

Figure 2. Propagation direction and polarization of the ordinary wave $\vec{E}_o$ and extraordinary wave $\vec{E}_e$ in SALC.

The corresponding linear electric induction vectors $\vec{D}_o^L, \vec{D}_e^L$ are given by [7, 18]

$$D_{oy}^L = \varepsilon_0 \varepsilon_\perp E_y; \vec{D}_e^L = \varepsilon_0 \left(\vec{a}_x \varepsilon_\perp e_{ex} + \vec{a}_z \varepsilon_\parallel e_{ez} \right) A_e \exp[i(k_{ex}x + k_{ez}z - \omega t)] + c.c. \tag{16}$$

In the linear approximation, substituting Eqs. (14)–(16) into the wave Eq. (13) we obtain the dispersion relations for the ordinary and extraordinary waves, respectively [7, 18]

$$k_o^2 = \varepsilon_\perp \frac{\omega^2}{c^2}; \frac{k_{ex}^2}{\varepsilon_\parallel} + \frac{k_{ez}^2}{\varepsilon_\perp} = \frac{\omega^2}{c^2} \tag{17}$$

It should be noted that the ordinary and extraordinary beams in the uniaxial medium propagate in different directions and the vectors $\vec{E}_e$ and $\vec{D}_e^L$ are not parallel [18]. The extraordinary wave propagates in the direction of the beam vector $\vec{s} \perp \vec{E}_e$, which is determined by the angle $\theta_e = \arctan\{(\varepsilon_\perp/\varepsilon_\parallel)\tan\theta_1\}$ with respect to the Z axis [18]. Here, θ_1 is the angle between $\vec{k}_e$ and the Z axis.

We consider separately the self-focusing and self-trapping of the ordinary and extraordinary beams [7]. We start with the analysis of the slab-shaped ordinary beam with the dimension in the Y direction much greater than in the incidence XZ plane. In such a case, the dependence on the coordinate y may be neglected [7, 9]. Substituting expression (14) into the equation of motion (9), we obtain [7, 9]

$$\frac{\partial u}{\partial z} = \frac{\varepsilon_0 a_\perp}{B} |A_o|^2; D_o^{NL} = \varepsilon_0 a_\perp \frac{\partial u}{\partial z} E_o \tag{18}$$

Expression (18) shows that the nonlinearity related to the smectic layer normal strain is the Kerr-type nonlinearity [14]. We introduce now the coordinates (x', z') parallel and normal to the ordinary beam propagation direction, respectively [7, 9]

$$x' = x\sin\theta_o + z\cos\theta_o; z' = -x\cos\theta_o + z\sin\theta_o \tag{19}$$

Here, θ_o is the angle between $\vec{k}_o$ and the Z axis. We use the SVAA for the ordinary beam amplitude A_o [14]

$$\left|\frac{\partial^2 A_o}{\partial x'^2}\right| \ll \left|k_o \frac{\partial A_o}{\partial x'}\right| \sim \left|\frac{\partial^2 A_o}{\partial z'^2}\right| \tag{20}$$

We are interested in the spatially localized solutions with the following boundary conditions [7, 9]

$$\lim_{z'\to\infty} |A_o(z')| = 0; \frac{\partial |A_o(z')|}{\partial z'}\bigg|_{z'=0} = 0; |A_o(z'=0)| = |A_o|_{\max} \tag{21}$$

Then, substituting expressions (14), (18), (19) and the first ones of Eq. (16), (17) into Eq. (13) and taking into account the SVAA conditions (20), we obtain the truncated equation for the SVA $A_o(x', z')$, which has the form [7]

$$i\frac{\partial A_o}{\partial x'} + \frac{1}{2k_o}\frac{\partial^2 A_o}{\partial z'^2} + \frac{\omega^2}{c^2}\frac{\varepsilon_0 a_\perp^2}{2Bk_o}|A_o|^2 A_o = 0 \tag{22}$$

Eq. (22) is the nonlinear Schrodinger equation (NSE) [19]. The coefficient of the last term in the left-hand side (LHS) of Eq. (22) is positive definite $\omega^2\varepsilon_0^2 a_\perp^2/\left(4c^2Bk_o\right) > 0$, which corresponds to the stationary two-dimensional self-focusing of the light beam. The solution of Eq. (22) with the boundary conditions (21) has the form [7]

$$A_o(x', z') = |A_o|_{\max}\exp\left(i\frac{\varepsilon_0 a_\perp^2 |A_o|_{\max}^2}{4B\varepsilon_\perp}k_o x'\right)\left[\cosh\left(\frac{\sqrt{\varepsilon_0}a_\perp |A_o|_{\max}}{\sqrt{2B\varepsilon_\perp}}k_o z'\right)\right]^{-1} \tag{23}$$

The self-trapped beam (23) is the so-called spatial soliton with the width $w_o = \sqrt{2B\varepsilon_\perp}\left(\sqrt{\varepsilon_0}a_\perp |A_o|_{\max}k_o\right)^{-1}$ [7].

The self-trapped ordinary beam normalized intensity spatial distribution is shown in **Figure 3**.

The self-trapping of the extraordinary beam (15) can be realized only when the anisotropy angle $(\theta_1 - \theta_e)$ is small enough: $\tan(\theta_1 - \theta_e) \ll (k_e w_o)^{-1}$ [7]. For the typical values of $\varepsilon_\perp, \varepsilon_\parallel$ [2], the following condition is valid: $0 \le \tan(\theta_1 - \theta_e) \le 0.12$, and the self-trapping condition for the extraordinary beam can be satisfied [7]. Then, using the procedure described above for the ordinary beam, we obtain the spatial soliton of the extraordinary beam. It has the form [7, 10]

$$A_e = |A_e|_{\max}\exp\left[i\frac{\varepsilon_0 h_e^2 |A_e|_{\max}^2 \omega^2}{4Bl_{e\parallel}\left(1 + \frac{\varepsilon_a}{\varepsilon_\perp}e_{ez}\sin\theta_e\right)c^2\sin^2\theta_e}x''\right]\left[\cosh\left(\frac{z''}{w_e}\right)\right]^{-1} \tag{24}$$

Here, $x'' = x\sin\theta_e + z\cos\theta_e; z'' = -x\cos\theta_e + z\sin\theta_e$ are the coordinates parallel and perpendicular to the beam vector, respectively,

http://dx.doi.org/10.5772/intechopen.70997

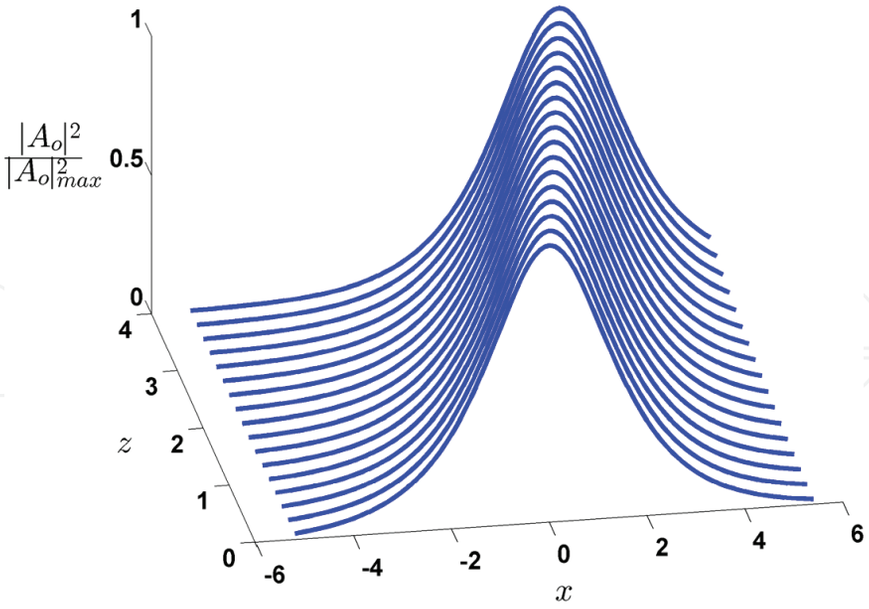

Figure 3. The self-trapped ordinary beam normalized intensity for the maximum amplitude $|A_o|_{\max} = 10^5 V/m$ and $\theta_o = \pi/6$.

$h_e = \left(a_\perp e_{ex}^2 + a_\parallel e_{ez}^2\right)\sin\theta_e + 2\varepsilon_a e_{ex} e_{ez}\cos\theta_e$, $l_{e\parallel} = k_{e\parallel}(1 + (\varepsilon_a/\varepsilon_\perp)\sin\theta_e)^{-1}$, and $k_{e\parallel}$ is the wave vector component parallel to the beam vector. The width w_e of the extraordinary beam spatial soliton is given by [7, 10]

$$w_e = \frac{\sqrt{2B\left(1 + \frac{\varepsilon_a}{\varepsilon_\perp} e_{ez}\sin\theta_e\right)}(\sin\theta_e)c}{\sqrt{\varepsilon_0} h_e |A_e|_{\max}\omega} \tag{25}$$

For the typical values of the SALC parameters [1, 2], the optical beam electric field $|A_{o,e}|_{\max}$ $\sim 10^5 V/m$, $\omega \sim 10^{15} s^{-1}$ and small angle θ_e the spatial soliton width is $w_{o,e} \sim 10^{-4} m$ [7]. SALC samples with a thickness of $10^{-4} m$ have been demonstrated experimentally [2, 17].

The optical wave self-trapping can occur also at the interface between the linear medium in the region $z < 0$ with the permittivity ε_s and the SALC cladding $(z > 0)$. For the light wave $E_y = A(z)\exp i(k_o x - \omega t)$ propagating along the interface parallel to the X axis, the self-trapped solution represents a bright surface wave with the amplitude $A(z)$ given by [7]

$$A(z) = A_{\max}\left[\cosh\left(\frac{z - z_0}{w_o}\right)\right]^{-1}; A_{\max} = A(z_0) \tag{26}$$

The cubic susceptibility of SALC $\chi^{(3)}_{SALC}$ related to the smectic layer compression is larger than $\chi^{(3)}$ related to the Kerr nonlinearity in organic liquids [14], but it is much less than the giant orientational nonlinearity (GON) in NLC [2]. However, the optical beam intensity in SALC may be much greater than in NLC, which are extremely sensitive to the strong optical fields [2]. In such cases, the approach based on the purely orientational mechanism of the optical nonlinearity is invalid.

4. Stimulated light scattering (SLS) in SALC

SLS is a process of parametric coupling between light waves and the material excitations of the medium [14]. We consider the SLS in SALC related to the smectic layer normal displacement and SS excited by the interfering optical waves [5, 6, 8–10]. We have taken into account the combined effect of SALC layered structure and anisotropy. It should be noted that SS propagates in SALC without the change of the mass density in such a way that the SS wave and the ordinary sound wave are decoupled [1].

In general case when the coupled optical waves have arbitrary polarizations and propagation directions, each optical wave in SALC ($z > 0$) splits into the extraordinary and ordinary ones with the same frequency and different wave vectors due to the strong anisotropy of SALC [6, 10, 18]. The polarizations of these waves are shown in **Figure 4**. The XZ plane is chosen to be the propagation plane of the waves $\vec{E}_1^{o,e}$. In such a case, the extraordinary wave $\vec{E}_1^{e}$ is polarized in the XZ plane, while the ordinary wave $\vec{E}_1^{o}$ is parallel to the Y axis [18]. The ordinary wave $\vec{E}_2^{o}$ is polarized in the XY plane perpendicular to the optical Z axis, and the extraordinary wave $\vec{E}_2^{e}$ possesses a three-dimensional polarization vector $\vec{e}_2^{e}$ [18]. The wave vectors $\vec{k}_{1,2}^{o}$ and $\vec{k}_1^{e}$ of these waves satisfy the dispersion relations (17) while the three-dimensional wave vector $\vec{k}_2^{e}$ satisfies the dispersion relation $\left(\left(k_{2x}^{e}\right)^2 + \left(k_{2y}^{e}\right)^2\right)\varepsilon_{\parallel}^{-1} + \left(k_{2z}^{e}\right)^2\varepsilon_{\perp}^{-1} = (\omega_2/c)^2$ [18]. The fundamental ordinary and extraordinary waves have the form, respectively

$$\begin{aligned}\vec{E}_1^{o,e} &= \vec{e}_1^{o,e}\left\{A_1^{o,e}(z)\exp i\left[\left(\vec{k}_1^{o,e}\cdot\vec{r}\right) - \omega_1 t\right] + c.c.\right\}\\ \vec{E}_2^{o,e} &= \vec{e}_2^{o,e}\left\{A_2^{o,e}(z)\exp i\left[\left(\vec{k}_2^{o,e}\cdot\vec{r}\right) - \omega_2 t\right] + c.c.\right\}\end{aligned} \tag{27}$$

Here, $\omega_1 > \omega_2$ and $\Delta\omega = \omega_1 - \omega_2 \ll \omega_1$. Each pair of the waves (27) has the same frequency, and for this reason, we define the nonlinear mixing of these waves as partially frequency degenerate FWM [6]. We assume that the complex amplitudes $A_{1,2}^{o,e}(z) = \left|A_{1,2}^{o,e}(z)\right|\exp i\gamma_{1,2}^{o,e}(z)$ are slowly varying along the optical axis Z: $\left|\partial^2 A_{1,2}^{o,e}/\partial z^2\right| \ll \left|k_{1,2z}^{o,e}\partial A_{1,2}^{o,e}/\partial z\right|$. As a result, the nonlinear two-wave mixing analyzed in Ref. [5] transforms into a partially degenerate FWM [6, 10]. We substitute the waves (27) into equation of motion (9). The interfering optical waves (27) with close frequencies $\omega_{1,2}$ create a dynamic grating of the smectic layer normal displacement $u(x, y, z, t)$ consisting of four propagating harmonics with the same frequency and different wave vectors. It has the form [6]

$$u(x,y,z,t) = \frac{i\varepsilon_0}{\rho}\sum_{j=1}^{4}\frac{\left(\Delta k_{j\perp}\right)^2 h_j M_j}{\left(\Delta k_j\right)^2 G_j\left(\Delta\omega, \Delta\vec{k}_j\right)}\exp i\left[\left(\Delta\vec{k}_j\cdot\vec{r}\right) - \Delta\omega t\right] + c.c. \tag{28}$$

http://dx.doi.org/10.5772/intechopen.70997

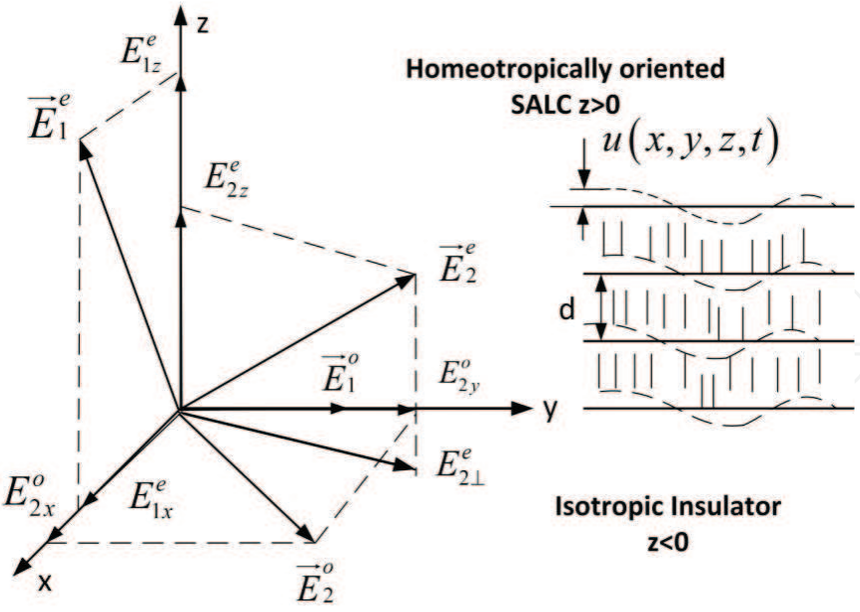

Figure 4. The polarizations of the fundamental ordinary waves $\vec{E}^o_{1,2}$ and extraordinary waves $\vec{E}^e_{1,2}$ in SALC (z > 0).

Here, $\Delta\vec{k}_1 = \vec{k}^e_1 - \vec{k}^o_2; \Delta\vec{k}_2 = \vec{k}^e_1 - \vec{k}^e_2; \Delta\vec{k}_3 = \vec{k}^o_1 - \vec{k}^o_2; \Delta\vec{k}_4 = \vec{k}^o_1 - \vec{k}^e_2;$

$h_1 = a_\perp \Delta k_{1z} e^e_{1x} e^o_{2x} - \varepsilon_a \left[\Delta k_{1x} e^e_{1z} e^o_{2x} + \Delta k_{1y} e^e_{1z} e^o_{2y}\right],$

$h_2 = a_\perp \Delta k_{2z} e^e_{1x} e^e_{2x} + a_\parallel \Delta k_{2z} e^e_{1z} e^e_{2z} - \varepsilon_a \left[\Delta k_{2x}\left(e^e_{1x} e^e_{2z} + e^e_{1z} e^e_{2x}\right) + \Delta k_{2y} e^e_{1z} e^e_{2y}\right]; h_3 = a_\perp \Delta k_{3z} e^o_{2y};$

$h_4 = a_\perp \Delta k_{4z} e^e_{2y} - \varepsilon_a \Delta k_{4y} e^e_{2z}; M_1 = A^e_1 \left(A^o_2\right)^*; M_2 = A^e_1 \left(A^e_2\right)^* M_3 = A^o_1 \left(A^o_2\right)^*,\ M_4 = A^o_1 \left(A^e_2\right)^*,$ and

$$G_j\left(\Delta\omega, \Delta\vec{k}_j\right) = (\Delta\omega)^2 + i\Delta\omega\Gamma_j - \Omega_j^2$$
$$\Gamma_j = \frac{1}{\rho}\left[\alpha_1 \frac{\left(\Delta k_{j\perp}\right)^2 \left(\Delta k_{jz}\right)^2}{\left(\Delta k_j\right)^2} + \frac{1}{2}(\alpha_4 + \alpha_{56})\left(\Delta k_j\right)^2\right]; \Omega_j^2 = s_0^2 \frac{\left(\Delta k_{j\perp}\right)^2 \left(\Delta k_{jz}\right)^2}{\left(\Delta k_j\right)^2} \tag{29}$$

The parametric amplification of the fundamental optical waves $\vec{E}^{o,e}_2$ with the lower frequency ω_2 by the other pair of optical waves $\vec{E}^{o,e}_1$ with the higher frequency ω_1 occurs in SALC due to the SLS on the light-induced smectic layer dynamic grating (28) [6, 10]. It is actually the Stokes SLS [14]. The fundamental optical waves also create Stokes and anti-Stokes small harmonics with the combination frequencies and wave vectors. The analysis of SLS in SALC is based on the simultaneous solution of the smectic layer equation of motion (9), the wave Eq. (13) for ordinary waves (14) and extraordinary waves (15) with the permittivity tensor (8). The nonlinear part of the permittivity tensor (8) ε^N_{ik} in the three-dimensional case can be written as follows [6]

$$\varepsilon^N_{ik} = \widehat{N}_{ik} u(x,y,z,t); \widehat{N}_{xx} = \widehat{N}_{yy} = a_\perp \frac{\partial}{\partial z}; \widehat{N}_{xy} = \widehat{N}_{yx} = 0;$$
$$\widehat{N}_{xz} = \widehat{N}_{zx} = -\varepsilon_a \frac{\partial}{\partial x}; \widehat{N}_{yz} = \widehat{N}_{zy} = -\varepsilon_a \frac{\partial}{\partial y}; \widehat{N}_{zz} = a_\parallel \frac{\partial}{\partial z} \tag{30}$$

Combining Eqs. (27)–(30), we obtain the nonlinear part of the electric induction, or the nonlinear polarization $D_i^{NL} = \varepsilon_0 \varepsilon_{ik}^N E_k$ [6]. This nonlinear polarization consists of two types of terms: (i) four harmonics, which are phase-matched with fundamental waves (27); (ii) all other terms with the combination frequencies and wave vectors, which give rise to the small scattered Stokes and anti-Stokes harmonics similar to the Brillouin scattering [6, 10, 14]. The combination of the anisotropy and nonlinearity also results in the creation of the small additional components of the waves $\vec{E}_1^{o,e}$ and $\vec{E}_2^{o}$ polarized in the XZ plane and XY plane, respectively [6].

We start with the analysis of the parametric coupling among the waves (27). Substituting expressions (27)–(30) and the phase-matched part of $\vec{D}^{NL}$ into wave Eq. (13), taking into account SVAA for the complex amplitudes $A_{1,2}^{o,e}(z)$, and separating the real and imaginary parts, we obtain the truncated equations for the magnitudes $\left|A_{1,2}^{o,e}(z)\right|$ and phases $\gamma_{1,2}^{o,e}(z)$ of these SVA [6]

$$2l_1^{o,e}\frac{\partial\left|A_1^{o,e}\right|}{\partial z} = -\left(\frac{\omega_1}{c}\right)^2 \times \frac{\varepsilon_0\Delta\omega}{\rho}\left\{\frac{h_{3,2}^2(\Delta k_{3,2\perp})^2\Gamma_{3,2}}{|G_{3,2}|^2(\Delta k_{3,2})^2}\left|A_2^{o,e}\right|^2 + \frac{h_{4,1}^2(\Delta k_{4,1\perp})^2\Gamma_{4,1}}{|G_{4,1}|^2(\Delta k_{4,1})^2}\left|A_2^{e,o}\right|^2\right\}\left|A_1^{o,e}\right| \tag{31}$$

$$2l_2^{o,e}\frac{\partial\left|A_2^{o,e}\right|}{\partial z} = \left(\frac{\omega_2}{c}\right)^2 \times \frac{\varepsilon_0\Delta\omega}{\rho}\left\{\frac{h_{3,2}^2(\Delta k_{3,2\perp})^2\Gamma_{3,2}}{|G_{3,2}|^2(\Delta k_{3,2})^2}\left|A_1^{o,e}\right|^2 + \frac{h_{1,4}^2(\Delta k_{1,4\perp})^2\Gamma_{1,4}}{|G_{1,4}|^2(\Delta k_{1,4})^2}\left|A_1^{e,o}\right|^2\right\}\left|A_2^{o,e}\right| \tag{32}$$

$$2l_1^{o,e}\frac{\partial\gamma_1^{o,e}}{\partial z} = -\left(\frac{\omega_1}{c}\right)^2\frac{\varepsilon_0}{\rho} \times \left\{\frac{h_{3,2}^2(\Delta k_{3,2\perp})^2\left[(\Delta\omega)^2 - \Omega_{3,2}^2\right]}{|G_{3,2}|^2(\Delta k_{3,2})^2}\left|A_2^{o,e}\right|^2 + \frac{h_{4,1}^2(\Delta k_{4,1\perp})^2\left[(\Delta\omega)^2 - \Omega_{4,1}^2\right]}{|G_{4,1}|^2(\Delta k_{4,1})^2}\left|A_2^{e,o}\right|^2\right\} \tag{33}$$

$$2l_2^{o,e}\frac{\partial\gamma_2^{o,e}}{\partial z} = -\left(\frac{\omega_2}{c}\right)^2\frac{\varepsilon_0}{\rho} \times \left\{\frac{h_{3,2}^2(\Delta k_{3,2\perp})^2\left[(\Delta\omega)^2 - \Omega_{3,2}^2\right]}{|G_{3,2}|^2(\Delta k_{3,2})^2}\left|A_1^{o,e}\right|^2 + \frac{h_{1,4}^2(\Delta k_{1,4\perp})^2\left[(\Delta\omega)^2 - \Omega_{1,4}^2\right]}{|G_{1,4}|^2(\Delta k_{1,4})^2}\left|A_1^{e,o}\right|^2\right\} \tag{34}$$

Here, $l_{1,2}^o = k_{1,2z}^o$; $l_{1,2}^e = k_{1,2z}^e\left[1 - e_{1,2z}^e\left(\vec{k}_{1,2}^e \cdot \vec{e}_{1,2}^e\right)\left(k_{1,2z}^e\right)^{-1}\right]$.

Eqs. (31) and (32) describe the parametric energy exchange between the fundamental waves, Eqs. (33) and (34) describe the cross-phase modulation (XPM) of these waves [6]. Combining Eqs. (31) and (32), we obtain the Manley-Rowe relation, which expresses the conservation of the total photon number [14]. In our case, it has the form [6]

$$\left(\frac{\omega_1}{c}\right)^{-2}\left[l_1^o\left|A_1^o\right|^2+l_1^e\left|A_1^e\right|^2\right]+\left(\frac{\omega_2}{c}\right)^{-2}\left[l_2^o\left|A_2^o\right|^2+l_2^e\left|A_2^e\right|^2\right]=const=I_0 \tag{35}$$

The solution of the system of Eqs. (31)–(34) can be written in the integral form [6, 10]

$$w_1^{o,e}=w_1^{o,e}(0)\exp\left\{-\int_0^z\left(\beta_{3,2}w_2^{o,e}+\beta_{4,1}w_2^{e,o}\right)dz'\right\} \tag{36}$$

$$w_2^{o,e}=w_2^{o,e}(0)\exp\left\{\int_0^z\left(\beta_{3,2}w_1^{o,e}+\beta_{1,4}w_1^{e,o}\right)dz'\right\} \tag{37}$$

$$\gamma_1^{o,e}-\gamma_1^{o,e}(0)=-\frac{1}{2}\int_0^z\left(\delta_{3,2}w_2^{o,e}+\delta_{4,1}w_2^{e,o}\right)dz' \tag{38}$$

$$\gamma_2^{o,e}-\gamma_2^{o,e}(0)=-\frac{1}{2}\int_0^z\left(\delta_{3,2}w_1^{o,e}+\delta_{1,4}w_1^{e,o}\right)dz' \tag{39}$$

Here, the dimensionless variables are given by [6]:

$$w_{1,2}^{o,e}=\frac{1}{I_0}\left(\frac{\omega_{1,2}}{c}\right)^{-2}l_{1,2}^{o,e}\left|A_{1,2}^{o,e}\right|^2;\ w_1^o+w_1^e+w_2^o+w_2^e=1 \tag{40}$$

$$\beta_j=C_j\Gamma_j\Delta\omega,\ \delta_j=C_j\left[(\Delta\omega)^2-\Omega_j^2\right],\ j=1,2,3,4,$$

$$C_j=\left(\frac{\omega_1\omega_2}{c^2}\right)^2\frac{\varepsilon_0 I_0\left(\Delta k_{j\perp}\right)^2}{\rho\left|G_j\right|^2 d_j\left(\Delta k_j\right)^2};\ d_1=l_1^el_2^o,\ d_2=l_1^el_2^e,\ d_3=l_1^ol_2^o,\ d_4=l_1^ol_2^e \tag{41}$$

Comparison of Eq. (36), (37), and (40) shows that for $z\to\infty$ $w_1^{o,e}\to 0$ and $w_2^o+w_2^e\to 1$. Hence, the pumping waves with the larger frequency ω_1 are depleted, the signal waves with smaller frequency $\omega_2<\omega_1$ are amplified with the saturation at the sufficiently large distances, and the system is stable. The gain terms β_j reach their maximal values close to the SS resonance condition $\Delta\omega\approx\Omega_j$, which can be satisfied for $\Delta\omega\sim\omega_1 s_0/c\ll\omega_1$ [6]. In such a case, $\beta_j\gg\delta_j$, the parametric amplification process is dominant while XPM can be neglected.

In general case, the exact analytical solution of Eqs. (31)–(34) is hardly possible. However, the explicit expressions for the coupled wave SVA have been obtained when both waves are propagating in the same XZ plane [5, 6]. For instance, assume that the pumping extraordinary wave with the frequency $\omega_1>\omega_2$ is mainly polarized in the XZ plane, the signal ordinary wave with the frequency ω_2 is mainly polarized along the Y axis, and the intensities of the components with other polarizations are small in such a way that $w_1^e\gg w_1^o;\ w_2^o\gg w_2^e$. Then, in the first approximation, the normalized intensities w_1^e, w_2^o of the main components have the form [6, 10]

$$w_1^e = \frac{1}{2}J_1\left[1-\tanh\left(\eta-\eta_0\right)\right]; w_2^o = \frac{1}{2}J_1\left[1+\tanh\left(\eta-\eta_0\right)\right] \tag{42}$$

Here, $w_1^e + w_2^o = J_1 = const = w_1^e(0) + w_2^o(0)$, $\eta = \beta_1 J_1 z/2$. It is seen from Eq. (42) that for $\eta \to \infty$ $w_1^e \to 0; w_2^o \to J_1$, and the crossing point $z_0 = \left(\beta_1 J_1\right)^{-1}\ln\left(w_1^e(0)/w_2^o(0)\right)$ exists only for $w_1^e(0)/w_2^o(0) > 1$. The coordinate dependence of the normalized intensities w_1^e, w_2^o is presented in **Figure 5**. The numerical estimations show that for the typical values of SALC parameters [1–3] in the resonant case the coupling constant per unit optical intensity $\beta_1/P_{opt} \sim (0.01 - 10)cm/MW$ [6]. For the optical intensity $P_{opt} \sim 10^6 - 10^7 Wcm^{-2}$, the SLS gain $\beta_{1\max} \sim 10^2 cm^{-1}$, which is at least an order of magnitude larger than the gain at Brillouin SLS in isotropic organic liquids [14]. Such optical intensities are feasible [20, 21].

The explicit expressions of the small component intensities w_1^o and w_2^e can be obtained in the second approximation. They have the form [6]

$$\begin{aligned} w_1^o &= w_1^o(0)\left\{\frac{\exp(-\eta)\cosh\left(\eta_0\right)}{\cosh\left(\eta-\eta_0\right)}\right\}^{\beta_3/\beta_1} \\ w_2^e &= w_2^e(0)\left\{\frac{\exp(\eta)\cosh\left(\eta_0\right)}{\cosh\left(\eta-\eta_0\right)}\right\}^{\beta_2/\beta_1} \end{aligned} \tag{43}$$

It is easy to see from Eq. (43) that for $\eta \to \infty$ $w_1^o \to 0$ and $w_2^e \to w_2^e(0)\left[1 + w_1^e(0)/w_2^o(0)\right]^{\beta_2/\beta_1}$ $= const$.

The evaluation of the phases $\gamma_{1,2}^{o,e}$ shows that the pumping wave phases $\gamma_1^{o,e}$ rapidly increase that results in the fast oscillations of the depleted amplitudes $A_1^{o,e}(z)$ [6]. The phases $\gamma_2^{o,e}$ of the signal waves tend to the constant values at sufficiently large η [6].

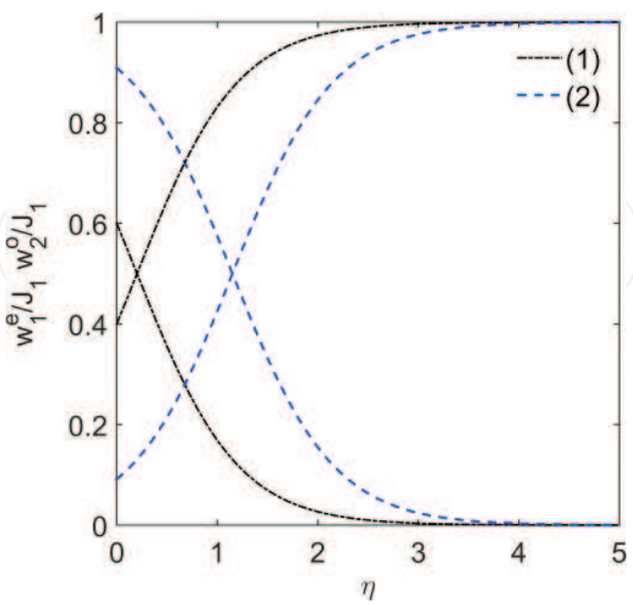

Figure 5. The dependence of the normalized pumping and signal intensities $w_1^e/J_1; w_2^o/J_1$ on the dimensionless coordinate η for the pumping-to-signal ratio $w_1^e(0)/w_2^o(0) = 1.5; 5$ (curves 1 and 2, respectively).

The Brillouin-like SLS also results in the generation of six Stokes small harmonics with the frequency $(\omega_2 - \Delta\omega)$ and combination wave vectors, six anti-Stokes small harmonics with the frequency $(\omega_1 + \Delta\omega)$ and combination wave vectors, and eight small harmonics with the fundamental frequencies $\omega_{1,2}$ and combination wave vectors [6].

5. The nondegenerate FWM in SALC

Consider now the nondegenerate FWM in SALC [8–10]. Assume that four coupled fundamental optical waves have different close frequencies ω_n such that $\Delta\omega_{mn} = \omega_m - \omega_n \sim s_0\omega_n/c \ll \omega_n$. For the sake of definiteness, we suppose that $\omega_1 < \omega_2 < \omega_3 < \omega_4$. These fundamental waves have the form [8–10]

$$\vec{E}_m = \vec{e}_m\left\{A_m(z)\exp i\left[\left(\vec{k}_m\cdot\vec{r}\right) - \omega t\right] + c.c.\right\}, m = 1, \ldots, 4 \tag{44}$$

The interfering waves (44) create a dynamic grating of the smectic layer normal displacement of the type (28), but this time each harmonic has a different frequency $\Delta\omega_{mn} = \omega_m - \omega_n$, $m, n = 1, \ldots, 4$. We discuss two cases: (i) all waves (44) are polarized in the directions perpendicular to the propagation plane and propagate as ordinary waves; (ii) all waves (44) are polarized in the propagation plane and behave as extraordinary waves [8–10]. Using the SVAA and the theory developed in the previous section, we obtain the truncated equations for the slowly varying magnitudes $|A_m(z)|$ and phases $\gamma_m(z)$ similar to Eqs. (31)–(34). The analysis of these equations shows that the wave with the lowest frequency ω_1 is amplified up to the saturation level determined by the integral of motion I_0 similar to the one from Eq. (35) [8–10]

$$I_0 = \sum_{m=1}^{4} l_m\left(\frac{\omega_m}{c}\right)^{-2}|A_m|^2 = const \tag{45}$$

Here, the factors l_m are defined above for the ordinary or extraordinary wave, respectively. Three other waves with the higher frequencies $\omega_{2,3,4}$ undergo the depletion like the pumping waves [8–10]. The depletion of the waves $\vec{E}_{2,3,4}$ is accompanied by the XPM with the rapidly increasing phases while the phase of the signal wave $\vec{E}_1$ saturates at large distances. The analytical solution of the type (42) and (43) has been obtained for the case when the pumping wave $\vec{E}_4$ and the signal wave $\vec{E}_1$ are much stronger than the idler waves $\vec{E}_{2,3}$ with the intermediate frequencies $\omega_{2,3}$ [8–10].

In the special case when some ordinary optical waves (44) have perpendicular polarizations vectors $\vec{e}_{m\perp}\perp\vec{e}_{n\perp}$ the polarization-decoupled FWM is possible [8–10]. Such waves do not excite the dynamic grating since the corresponding coupling constants $h^o_{mn} = a_\perp\Delta k_{mnz}\left(\vec{e}_{m\perp}\cdot\vec{e}_{n\perp}\right)$ vanish [8–10]. In the case of the extraordinary wave mixing, the polarization-decoupled FWM is impossible because of the SALC anisotropy. If the electric field of the signal ordinary wave $\vec{E}_1$ is perpendicular to the fields of all other waves than this wave propagates though SALC

without any change of its SVA: $A_1^o = const$. If $\vec{E}_1^o \perp \vec{E}_{2,3}^o$ and $\vec{E}_1^o \| \vec{E}_4^o$, then FWM is divided in two separate two-wave mixing processes between the waves $\vec{E}_{1,4}^o$ and the waves $\vec{E}_{2,3}^o$ with the solutions similar to solution (42) [8].

In the important case when the pumping wave $\vec{E}_4$ and the signal wave $\vec{E}_1$ are much stronger than the idler waves $\vec{E}_{2,3}$, the approximate solution can be obtained similarly to the solution (42) and (43) in the case of SLS [8–10]. It has been shown that this solution is stable in the case of FWM [8].

In the particular case when the fundamental waves (44) are counter-propagating, the phase conjugation is possible as a result of the nondegenerate FWM in SALC [8–10]. Optical phase conjugation (OPC) is the wavefront reversion property of a backward propagating optical wave with respect to a forward propagating wave [22]. The optical waves are phase conjugated to each other if their complex amplitudes are conjugated with respect to their phase factors [22]. Typically, OPC results from nonlinear optical processes such as FWM and SLS [20]. LC are commonly used for FWM and OPC [22].

Suppose that the waves $\vec{E}_{1,4}$ are phase-conjugate while the waves $\vec{E}_{2,3}$ are forward-going and backward-going pumping waves, which have the form [8]

$$\begin{aligned}
\vec{E}_1 &= \vec{e}_1\left\{A_1 \exp i\left[\left(\vec{k}_4 \cdot \vec{r}\right) + \omega_1 t\right] + c.c.\right\} \\
\vec{E}_2 &= \vec{e}_2\left\{A_2 \exp i\left[\left(\vec{k}_2 \cdot \vec{r}\right) - \omega_2 t\right] + c.c.\right\} \\
\vec{E}_3 &= \vec{e}_3\left\{A_3 \exp i\left[\left(\vec{k}_2 \cdot \vec{r}\right) + \left(\Delta \vec{k} \cdot \vec{r}\right) + \omega_3 t\right] + c.c.\right\} \\
\vec{E}_4 &= \vec{e}_4\left\{A_4 \exp i\left[\left(\vec{k}_4 \cdot \vec{r}\right) - \omega_4 t\right] + c.c.\right\}
\end{aligned} \tag{46}$$

Here, $\Delta \vec{k} = \Delta \vec{k}_{32}$ is the wave vector mismatch of the FWM process. In the case of OPC caused by SLS the frequency balance condition between the waves with the same vectors is necessary. We assume that $\omega_3 - \omega_1 = \omega_4 - \omega_2$. Suppose that the pumping waves $\vec{E}_{2,3}$ are much stronger than the probe wave $\vec{E}_4$ and the phase-conjugate wave $\vec{E}_1$ propagating in the negative direction as it is seen from Eq. (46). In such a case, using the constant pumping approximation (CPA) [14] where $A_{2,3} = const$, we obtain the following solution for the probe wave and the phase-conjugate wave SVA $A_{1,4}$ [8–10]

$$A_{1,4} = A_{01,4} \exp\left[gr \pm \frac{i}{2}\left(\Delta \vec{k} \cdot \vec{r}\right)\right] \tag{47}$$

Analysis of the truncated equations for $A_{1,4}$ shows that there exists the solution with the gain $\mathrm{Re} g < 0$ corresponding to the amplification of the phase-conjugate wave $\vec{E}_1$ [8–10]. Such a case can be characterized as a kind of the Brillouin-enhanced FWM (BEFWM) based on the optical nonlinearity related to the smectic layer normal displacement [8–10]. Numerical estimations show that the amplification of the phase-conjugate wave $\vec{E}_1$ is possible for the typical values of

http://dx.doi.org/10.5772/intechopen.70997

SALC parameters and for the pumping wave intensity of about 100 $MWcm^{-2}$ [9], which is feasible [20, 21]. OPC in the homeotropically oriented SALC film with the thickness of 250 μm had been demonstrated experimentally [20].

The components of the nonlinear electric induction $\vec{D}^{NL}$, which are not phase matched to the fundamental waves (46) give rise to 12 doubly degenerate combination harmonics of the type. $A_m A_p A_n^* \exp i\left[\left(\left(\vec{k}_m + \vec{k}_p - \vec{k}_n\right)\cdot \vec{r}\right) - \left(\omega_m + \omega_p - \omega_n\right)t\right]$ and 12 harmonics of the type $A_m^2 A_n^* \exp i\left[2\left(\left(\vec{k}_m \cdot \vec{r}\right) - \omega_m t\right) - \left(\vec{k}_n \cdot \vec{r}\right) + \omega_n t\right]$ [8–10].

6. Nonlinear interaction of surface plasmon polaritons (SPP) in SALC

Integration of strongly nonlinear LC with plasmonic structures and metamaterials would enable active switching and tuning operations with low threshold [4]. LC may be also used in reconfigurable metamaterials for tuning the resonant frequency, the transmission/ reflection coefficient, and the refractive index [23]. Combination of metamaterials and active plasmonic structures with NLC has been investigated [4, 23]. In this section, we discuss the nonlinear optical effects caused by the SPP mixing in SALC, which is characterized by low losses and a strong nonlinearity related to the smectic layer normal displacement without the change of the mass density [11–13]. Consider the interface $z = 0$ between a homeotropically oriented SALC $(z > 0)$ and a metal $(z < 0)$ shown in **Figure 6** [11, 12]. The SALC optical Z axis and the X axis are chosen to be perpendicular and parallel to the interface $z = 0$, respectively.

SPP from the metal penetrate into SALC. The permittivity of the metal $\varepsilon_m(\omega)$ determined by the Drude model is given by $\varepsilon_m(\omega) = 1 - \omega_p^2 \omega^{-1}(\omega + (i/\tau))^{-1}$ where $\omega_p = \sqrt{n_0 e^2/(\varepsilon_0 m)}$ is the plasma frequency, n_0 is the free electron density in the metal, e, m are the electron charge and mass, respectively, ω, τ are the SPP angular frequency and lifetime, respectively [24, 25]. The efficient SLS in SALC takes place for the counter-propagating SPP with close frequencies

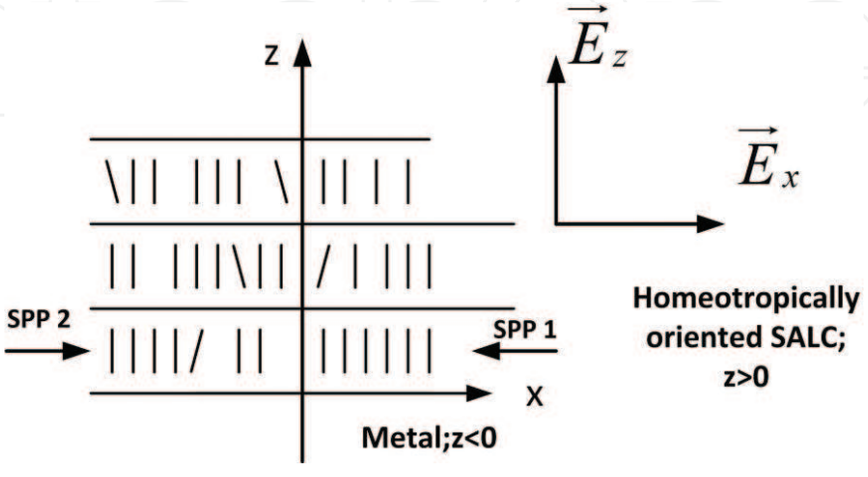

Figure 6. The counter-propagating SPP at the interface between a metal $(z < 0)$ and a homeotropically oriented SALC $(z > 0)$.

$\omega_1 > \omega_2$ such that $\Delta\omega = \omega_1 - \omega_2 \ll \omega_1$ [12]. The spatially localized electric fields of these SPP in SALC have the form [24, 25]

$$\vec{E}_{1,2} = \frac{1}{2}\left\{\vec{e}_{1,2}A_{1,2}(x,t)\exp\left[\pm ik_x(x \pm d) - k_z^S z - i\omega_{1,2}t\right] + c.c.\right\} \tag{48}$$

The SPP are polarized as transverse magnetic (TM) waves with the electric field components $E_{x,z}$ and the magnetic field component H_y [23, 24]. In an optically uniaxial SALC, SPP propagate as extraordinary waves [18]. The numerical estimations show that for the optical frequency range and the small frequency difference $\Delta\omega \approx \left(10^{-7} - 10^{-5}\right)\omega_1$ the $\mathrm{SPP}_{1,2}$ wave vectors are practically equal [11, 12]. They have the form [11, 12]

$$\begin{aligned} k_z^S &= \sqrt{k_x^2\left(\varepsilon_\perp/\varepsilon_\parallel\right) - \omega_1^2\varepsilon_\perp/c^2} \\ k_x &= (\omega_1/c)\sqrt{\varepsilon_m(\omega_1)[1 - (\varepsilon_m(\omega_1)/\varepsilon_\perp)]\left[1 - \left(\varepsilon_m^2(\omega_1)/\left(\varepsilon_\perp\varepsilon_\parallel\right)\right)\right]^{-1}} \end{aligned} \tag{49}$$

Numerical estimations show that for the typical values of $\omega_{1,2}$, ω_p, τ the following relations are valid: $\mathrm{Re}k_z^S \gg \mathrm{Im}k_z^S$, $\mathrm{Re}k_x \gg \mathrm{Im}k_x$ [11, 12, 24, 25]. For the optical wavelength $\lambda_{opt} \approx (0.6 - 1.33)\mu m$, the SPP propagation length L_x and the wavelength λ_s are given by, respectively: $L_x = (\mathrm{Im}k_x)^{-1} \approx (84 - 550)\mu m$, $\lambda_s = 2\pi/(\mathrm{Re}k_x) \approx (0.33 - 0.77)\mu m \ll L_x$ [12]. The SPP localization length $L_z = \left(\mathrm{Re}k_z^S\right)^{-1} \sim 10^{-6}m$ belongs to the subwavelength scale: $\mathrm{Im}k_z^S \sim 10m^{-1} \ll \mathrm{Re}k_z^S$ and can be neglected [12].

Substituting the SPP fields (48) into the smectic layer equation of motion (9), we obtain the dynamic grating $u(x,z,t)$ given by [11, 12]

$$u(x,z,t) = 0.5\left[U\exp\left\{i(2\mathrm{Re}k_x)x - 2(\mathrm{Im}k_x)d - \left(2\mathrm{Re}k_z^S\right)z - i\Delta\omega t\right\} + c.c.\right] \tag{50}$$

Here,

$$U = -\frac{\varepsilon_0(2\mathrm{Re}k_x)^2 hA_1(x,t)A_2^*(x,t)}{\rho\left[-(2\mathrm{Re}k_x)^2 + \left(2\mathrm{Re}k_z^S\right)^2\right]G\left(k_x, k_z^S, \Delta\omega\right)} \tag{51}$$

$$\begin{aligned} h &= -\left(2\mathrm{Re}k_z^S\right)\left(-a_\perp|e_{1x}|^2 + a_\parallel|e_{1z}|^2\right) - 4\varepsilon_a(2\mathrm{Re}k_x)\mathrm{Im}\left(e_{1z}e_{1x}^*\right); \\ G\left(k_x, k_z^S, \Delta\omega\right) &= (\Delta\omega)^2 - \frac{B(2\mathrm{Re}k_x)^2\left(2\mathrm{Re}k_z^S\right)^2}{\rho\left[-(2\mathrm{Re}k_x)^2 + \left(2\mathrm{Re}k_z^S\right)^2\right]} \\ &\quad -i\frac{\Delta\omega}{\rho}\left[-\alpha_1\frac{(2\mathrm{Re}k_x)^2\left(2\mathrm{Re}k_z^S\right)^2}{\left[-(2\mathrm{Re}k_x)^2 + \left(2\mathrm{Re}k_z^S\right)^2\right]} + \frac{(\alpha_4 + \alpha_{56})\left[-(2\mathrm{Re}k_x)^2 + \left(2\mathrm{Re}k_z^S\right)^2\right]}{2}\right] \end{aligned} \tag{52}$$

Unlike the dynamic grating (28) created by the interfering optical waves, the grating (50) caused by SPP is spatially localized both in the X and in the Z directions [11, 12]. The localized

grating (50) can be characterized as an enhanced Rayleigh wave of SS [26]. Analysis of $G\left(k_x, k_z^S, \Delta\omega\right)$ (52) shows that the resonant case $\mathrm{Re}G\left(k_x, k_z^S, \Delta\omega\right) = 0$ cannot be achieved for the frequency difference $\Delta\omega \sim \left(10^7 - 10^8\right)s^{-1}$, and the spontaneous SS surface wave can be neglected [12]. The cubic susceptibility of the SALC-metal system $\chi_{ijkl}^{(3)}(\Delta\omega); i, j, k, l = x, z$ related to the localized grating (50) is essentially complex. For the typical values of the SALC parameters, SPP in silver, $\omega_1 = 1.4 \times 10^{15}s^{-1}$ and $\Delta\omega \sim \left(10^7 - 10^8\right)s^{-1}$ the numerical estimations yield $\left|\chi_{xxxx}^{(3)}\right| \approx \left|\chi_{zzzz}^{(3)}\right| \sim \left(10^{-20} - 10^{-19}\right)m^2/V^2$ [11], which is larger by one-two orders of magnitude than the cubic susceptibilities of some organic liquids and solid materials [27].

We substitute the localized layer displacement $u(x, z, t)$ (50) into the expression of the SALC nonlinear permittivity (30), evaluate the nonlinear part of the electric induction $\vec{D^{NL}}$ for SPP (48), and by using the standard procedure, we obtain from Eq. (13) the truncated equations for the SPP SVA $A_{1,2}(t) = |A_{1,2}(t)|\exp i\gamma_{1,2}(t)$. The dependence of SVA $A_{1,2}$ on the x coordinate can be neglected in the central part of the dynamic grating (50) for the distances of several SPP wavelengths [12]. Integrating the SPP electric field and nonlinear electric induction over $z \in [0, \infty]$, we obtain the following truncated equations for the normalized SPP intensities $I_{1,2} = \left(|A_{1,2}|^2/\omega_{1,2}\right)I_0^{-1}$.

$$\frac{\partial I_{1,2}}{\partial t} = \mp g I_1 I_2 \tag{53}$$

Here, $\left(|A_1|^2/\omega_1\right) + \left(|A_2|^2/\omega_2\right) = I_0 = const$ is the integral of motion obtained from the Manley-Rowe relation [14], and the gain g has the form [12]

$$g = \frac{\varepsilon_0(2\mathrm{Re}k_x)^2 hb\mathrm{Im}\left\{G\left(k_x, k_z^S, \Delta\omega\right)\right\}I_0\omega_1\omega_2\exp(-2)}{6\rho\left(\varepsilon_\perp|e_x|^2 + \varepsilon_\parallel|e_z|^2\right)\left[(2\mathrm{Re}k_x)^2 - \left(2\mathrm{Re}k_z^S\right)^2\right]\left|G\left(k_x, k_z^S, \Delta\omega\right)\right|^2} > 0 \tag{54}$$

Here, $b = -2\mathrm{Re}k_z^S\left(-a_\perp|e_{1x}|^2 + a_\parallel|e_{1z}|^2\right) + 4\varepsilon_a(\mathrm{Re}k_x)\mathrm{Im}\left(e_{1z}e_{1x}^*\right)$. Solution of Eq. (53) has the form [12]

$$I_1(t) = \frac{I_1(0)}{I_1(0) + [1 - I_1(0)]\exp(-gt)}; I_2(t) = \frac{[1 - I_1(0)]\exp(-gt)}{I_1(0) + [1 - I_1(0)]\exp(-gt)} \tag{55}$$

It is easy to see from Eq. (55) that $I_1(t) + I_2(t) = 1$.

Expressions (55) show that the energy exchange between SPP takes place. In the limiting case $t \to \infty$, we obtain: $I_1(t) \to 1; I_2(t) \to 0$ [12]. The time dependence of the normalized SPP intensities $I_1(t), I_2(t)$ (55) is presented in **Figure 7**. The phases $\gamma_{1,2}(0)$ of the SPP SVA have the form

$$\gamma_1(t)-\gamma_1(0)=\frac{\mathrm{Re}\{G(k_x,k_z^S,\Delta\omega)\}}{2\mathrm{Im}\{G(k_x,k_z^S,\Delta\omega)\}}\ln\left[(1-I_1(0))\exp(-gt)+I_1(0)\right] \tag{56}$$

$$\gamma_2(t)-\gamma_2(0)=-\frac{\mathrm{Re}\{G(k_x,k_z^S,\Delta\omega)\}}{2\mathrm{Im}\{G(k_x,k_z^S,\Delta\omega)\}}\ln\left[I_1(0)\exp(gt)+1-I_1(0)\right] \tag{57}$$

It is easy to see from Eqs. (56) and (57) that for $t\to\infty$ the phase $\gamma_1(t)$ of the amplified SPP I_1 tends to a constant value $\gamma_1(t)-\gamma_1(0)\to\frac{\mathrm{Re}\{G(k_x,k_z^S,\Delta\omega)\}}{2\mathrm{Im}\{G(k_x,k_z^S,\Delta\omega)\}}\ln[I_1(0)]$, while the phase of the depleted SPP I_2 $\gamma_2(t)-\gamma_2(0)$ for large time intervals such that $gt\gg1$ takes the form $\gamma_2(t)-\gamma_2(0)\to-\frac{\mathrm{Re}\{G(k_x,k_z^S,\Delta\omega)\}}{2\mathrm{Im}\{G(k_x,k_z^S,\Delta\omega)\}}gt$ and $\gamma_2(t)\to-\infty$ for $t\to\infty$. The SVA of the depleted SPP I_2 undergoes strong XPM and rapidly oscillates in the time domain. The results (55)–(57) show that the Rayleigh stimulated scattering [27] of SPP on the smectic layer normal displacement localized grating is accompanied by XPM and the parametric energy exchange between SPP [12]. The rise time of the amplified SPP is about $1-2\mu s$ as it is seen from **Figure 7**. It is much faster than the thermal response time $\tau_R=100\,\mu s$ and the purely orientational response time $\approx25\,ms$ in NLC [4]. Numerical estimations show that for the SPP electric field of $10^7V/m$ the rise time of about 10 ns can be achieved, which is much less than the Brillouin relaxation time $\tau_B\approx200\,ns$ [4, 12].

Structures consisting of alternative conducting and dielectric thin films are capable of guiding SPP light waves [24, 25]. Each single interface can sustain bound SPP. When the distance between adjacent interfaces is comparable or smaller than the SPP localization length $L_z=\left(\mathrm{Re}k_z^S\right)^{-1}$, the coupled modes occur due to the interaction between SPP [24]. The following specific three-layer guiding systems can be considered: (i) an insulator/metal/insulator (IMI) heterostructure where a thin metallic layer is sandwiched between two infinitely thick dielectric claddings; (ii) a metal/insulator/metal (MIM) heterostructure where a thin dielectric core layer is sandwiched between two infinitely thick metallic claddings [24]. LC can be used as a tunable cladding material or as the guiding core material due to their excellent electro-optic properties

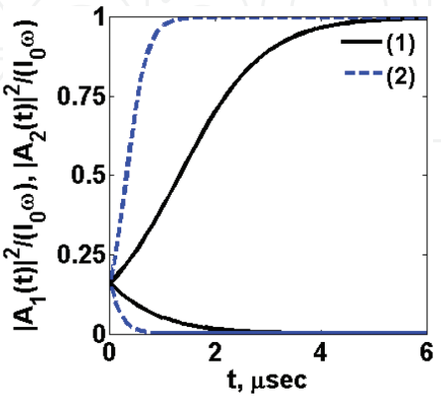

Figure 7. The temporal dependence of the SPP normalized intensities $I_{1,2}(t)$ for the input electric field of $10^6V/m$ and optical wavelengths $\lambda_{opt1}=0.6\mu m$ (curves 1) and $\lambda_{opt1}=1.33\mu m$ (curve 2).

and large nonlinearity [28]. Photonic components based on plasmonic waveguides with NLC core have been theoretically investigated in a number of articles (see, for example, [28–31] and references therein).

We consider the nonlinear optical processes in an MIM waveguide with the SALC core [13]. The structure of such a waveguide is shown in **Figure 8**. SPP propagating in the metal claddings and in SALC core are TM waves [24, 25]. The SPP electric and magnetic fields in the metallic claddings $z > d; z < -d$ $\vec{H}_{1,2}(x,z,t)$, $\vec{E}_{1,2}(x,z,t)$, and in the SALC core $|z| \le d$ $\vec{H}_{SA}(x,z,t)$, $\vec{E}_{SA}(x,z,t)$ have the form, respectively [24]

$$\vec{H}_{1,2}(x,z,t) = \frac{1}{2}\vec{a}_y H_{1,20}\exp\left(\mp k_z^m z + ik_x x - i\omega t\right) + c.c., |z| > d \tag{58}$$

$$\vec{E}_{1,2}(x,z,t) = \frac{1}{2}\left[\vec{a}_x E_{1,2x0} + \vec{a}_z E_{1,2z0}\right]\exp\left(\mp k_z^m z + ik_x x - i\omega t\right) + c.c., |z| > d \tag{59}$$

$$\vec{H}_{SA}(x,z,t) = \frac{1}{2}\vec{a}_y\left[A\exp\left(k_z^S z\right) + B\exp\left(-k_z^S z\right)\right]\exp(ik_x x - i\omega t) + c.c., |z| \le d \tag{60}$$

$$\begin{aligned}&\vec{E}_{SA}(x,z,t)\\ &= \frac{1}{2}\left\{\vec{a}_x \frac{k_z^S}{i\omega\varepsilon_0\varepsilon_\perp}\left[A\exp\left(k_z^S z\right) - B\exp\left(-k_z^S z\right)\right] - \vec{a}_z \frac{k_x}{\omega\varepsilon_0\varepsilon_\parallel}\left[A\exp\left(k_z^S z\right) + B\exp\left(-k_z^S z\right)\right]\right\}\\ &\times\exp i(k_x x - \omega t) + c.c.; |z| \le d\end{aligned} \tag{61}$$

The complex wave number k_z^S of SPP in SALC in the linear approximation is determined by expression (49) and the SPP wave number in the metallic claddings is given by $k_z^m = \sqrt{k_x^2 - \varepsilon_m(\omega)\omega^2/c^2}$ [24]. Using the boundary conditions for the tangential components of the SPP fields (58)–(61) at the interface $z = d$ between the metallic cladding and the SALC core, we obtain the dispersion relation for the MIM modes [13, 24]

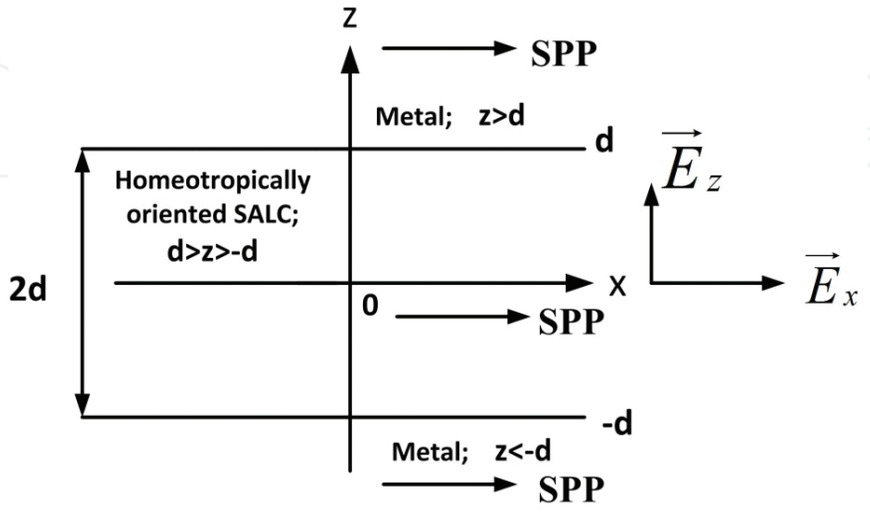

Figure 8. The MIM waveguide with the homeotropically oriented SALC as a core.

$$\exp\left(-4k_z^S d\right) = \left(\frac{k_z^m}{\varepsilon_r(\omega)} + \frac{k_z^S}{\varepsilon_\perp}\right)^2 \left(\frac{k_z^m}{\varepsilon_r(\omega)} - \frac{k_z^S}{\varepsilon_\perp}\right)^{-2} \tag{62}$$

Numerical estimations show that for the typical values of the SPP frequency ω, the plasma frequency ω_p, the SPP lifetime τ mentioned above, and the MIM thickness $2d = 1\mu m$ the following relationships take place:

$\mathrm{Re}k_z^S \sim 10^6 m^{-1} \gg \mathrm{Im}k_z^S \sim 10^4 m^{-1}$, $\mathrm{Re}k_x \sim 10^7 m^{-1} \gg \mathrm{Im}k_x \sim 10^3 m^{-1}$. The SPP wavelength in the Z direction is given by $2\pi\left(\mathrm{Im}k_z^S\right)^{-1} \sim 10^2 \mu m$ and can be neglected inside the MIM waveguide core with the thickness of $2d \sim 1\mu m$. Then, a single localized TM can exist in the MIM waveguide according to the dispersion relation (62). The even TM mode has the form [13]

$$\vec{E}_{SA} = E_0 \left[\vec{a}_x \cosh\left(k_z^S z\right) - \vec{a}_z i \frac{k_x \varepsilon_\perp}{k_z^S \varepsilon_\parallel} \sinh\left(k_z^S z\right)\right] \exp[i(k_x x - \omega t)] + c.c. \tag{63}$$

The distribution of the TM even mode normalized intensity $\left|\vec{E}_{SA}\right|^2 / |E_0|^2$ in the MIM waveguide core is presented in **Figure 9**. It is seen from **Figure 9** that the intensity is filling the MIM waveguide core due to the overlapping of SPP inserted from the metallic claddings $z < -d; z > d$. Substituting the SPP field (63) into equation of motion (9), we obtain the smectic layer normal strain [13].

$$\frac{\partial u}{\partial z} = \frac{\varepsilon_0 |E_0|^2}{B} \exp[-2(\mathrm{Im}k_x)x] \left\{ a_\perp \left|\cosh\left(k_z^S z\right)\right|^2 + a_\parallel \frac{|k_x|^2 \varepsilon_\perp^2}{\left|k_z^S\right|^2 \varepsilon_\parallel^2} \left|\sinh\left(k_z^S z\right)\right|^2 \right\} \tag{64}$$

The nonlinear polarization in the SALC core caused by the smectic layer strain (64) has the form [13]

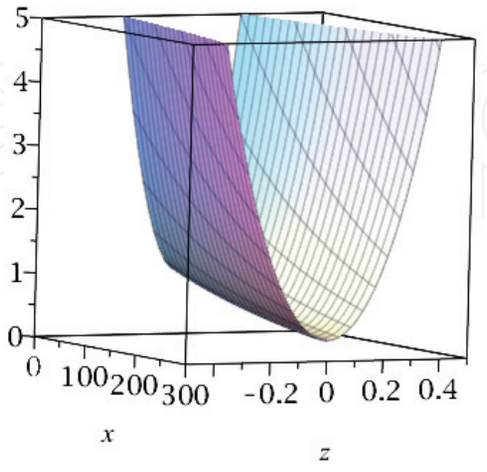

Figure 9. Distribution of the SPP normalized intensity $\left|\vec{E}_{SA}\right|^2 / |E_0|^2$ in the MIM waveguide core (arbitrary units).

$$\vec{D}_{SA}^{NL} = \varepsilon_0 \frac{\partial u}{\partial z} E_0 \left[\vec{a}_x a_\perp \cosh\left(k_z^S z\right) - \vec{a}_z i a_\parallel \frac{k_x \varepsilon_\perp}{k_z^S \varepsilon_\parallel} \sinh\left(k_z^S z\right) \right] \exp[i(k_x x - \omega t)] + c.c. \tag{65}$$

Substituting the SPP electric field (63) and nonlinear polarization (65) into Eq. (13) and separating linear and nonlinear parts, we obtain the truncated equation for SVA $E_0(t) = |E_0(t)| \exp i\varphi(t)$.

$$\begin{aligned} &-2i \frac{\partial E_0}{\partial t} E_0^* \varepsilon_\perp \left[\left|\cosh\left(k_z^S z\right)\right|^2 + \frac{|k_x|^2 \varepsilon_\perp}{\left|k_z^S\right|^2 \varepsilon_\parallel} \left|\sinh\left(k_z^S z\right)\right|^2 \right] \\ &= \omega \frac{\varepsilon_0 |E_0|^4}{B} \exp[-2(\mathrm{Im} k_x) x] \left[a_\perp \left|\cosh\left(k_z^S z\right)\right|^2 + a_\parallel \frac{|k_x|^2 \varepsilon_\perp^2}{\left|k_z^S\right|^2 \varepsilon_\parallel^2} \left|\sinh\left(k_z^S z\right)\right|^2 \right]^2 \end{aligned} \tag{66}$$

At the distances $x \ll L_x = (\mathrm{Im} k_x)^{-1}$, the SVA dependence on x can be neglected since $\exp[-2(\mathrm{Im} k_x)x] \approx 1$ [13]. The dispersion effects can be neglected because the dispersion length $L_D \gg L_x$ [13]. Integrating both sides of Eq. (66) over $z \in [-d, d]$ and separating real and imaginary parts we obtain the following equations for the magnitude $|E(t)|$ and phase $\varphi(t)$ of the SPP SVA.

$$\frac{\partial |E_0|^2}{\partial t} = 0; \frac{\partial \varphi}{\partial t} = \omega \frac{\varepsilon_0 |E_0|^2}{16B} \frac{F_2\left(k_z^S, k_x, d\right)}{F_1\left(k_z^S, k_x, d\right)} \tag{67}$$

Here,

$$\begin{aligned} F_1\left(k_z^S, k_x, d\right) &= \varepsilon_\perp \left[\left(1 + \frac{\varepsilon_\perp |k_x|^2}{\varepsilon_\parallel \left|k_z^S\right|^2}\right) \sinh\left[2\left(\mathrm{Re} k_z^S\right) d\right] + \left(1 - \frac{\varepsilon_\perp |k_x|^2}{\varepsilon_\parallel \left|k_z^S\right|^2}\right) 2\left(\mathrm{Re} k_z^S\right) d \right] \\ F_2\left(k_z^S, k_x, d\right) &= \left(a_\perp + a_\parallel \frac{\varepsilon_\perp^2 |k_x|^2}{\varepsilon_\parallel^2 \left|k_z^S\right|^2}\right)^2 \sinh\left[4\left(\mathrm{Re} k_z^S\right) d\right] \\ &+ 8\left(a_\perp^2 - \left(a_\parallel \frac{\varepsilon_\perp^2 |k_x|^2}{\varepsilon_\parallel^2 \left|k_z^S\right|^2}\right)^2\right) \sinh\left[2\left(\mathrm{Re} k_z^S\right) d\right] \\ &+ 8\left[\frac{1}{2}\left(a_\perp + a_\parallel \frac{\varepsilon_\perp^2 |k_x|^2}{\varepsilon_\parallel^2 \left|k_z^S\right|^2}\right)^2 + \left(a_\perp - a_\parallel \frac{\varepsilon_\perp^2 |k_x|^2}{\varepsilon_\parallel^2 \left|k_z^S\right|^2}\right)^2\right] \left(\mathrm{Re} k_z^S\right) d \end{aligned} \tag{68}$$

The solution of Eq. (67) has the form

$$|E_0|^2 = const; \varphi(t) = \left\{ \omega \frac{\varepsilon_0 |E_0|^2}{16B} \frac{F_2\left(k_z^S, k_x, d\right)}{F_1\left(k_z^S, k_x, d\right)} \right\} t \tag{69}$$

Eq. (69) shows that the strong SPM of the even SPP mode in the MIM wave guide occurs. It is enhanced by a large geometric factor $F_2\left(k_z^S, k_x, d\right) / F_1\left(k_z^S, k_x, d\right)$, which can achieve a value of $10^2 - 10^4$ for $2d = 1\mu m$ and $\mathrm{Re} k_z^S \sim \left(10^6 - 3 \times 10^6\right) m^{-1}$, $\mathrm{Re} k_x \sim \left(5 \times 10^6 - 10^7\right) m^{-1}$.

7. Conclusions

In SALC, there exists a specific mechanism of the optical nonlinearity related to the normal displacement $u(x, y, z, t)$ of smectic layers. This mechanism combines the properties of the orientational mechanism typical for LC and of the electrostrictive mechanism. In particular, the smectic layer oscillations occur without the mass density change. Under the resonant condition (11), the SS acoustic wave propagates in SALC in the direction oblique to the layer plane. The cubic nonlinearity related to this mechanism is characterized by a strong anisotropy, a short time response, a weak temperature dependence, a resonant frequency dependence, and a strong dependence on the optical wave polarization and propagation direction. The cubic susceptibility related to the smectic layer displacement is larger than the Kerr type susceptibility in ordinary organic liquids. It should be noted that the nonlinear optics of NLC has been mainly studied. However, SALC are promising candidates for nonlinear optical applications due to their low losses and higher degree of the long range order.

We derived the equation of motion (9) of the smectic layer displacement $u(x, y, z, t)$ in the electric field of optical waves. We investigated theoretically the nonlinear optical phenomena in SALC based on this specific mechanism. We solved simultaneously the equation of motion (9) and the wave Eq. (13) for the optical waves including the nonlinear polarization. The solution was based on the SVAA.

In an optically uniaxial SALC, an ordinary wave and an extraordinary one can propagate. Both the ordinary and extraordinary optical beams propagating in SALC undergo self-focusing and self-trapping and form spatial solitons. The optical wave self-trapping can occur at the interface between the linear medium and SALC. We obtained the analytical solutions for the SVA of the self-trapped beams.

SLS of two arbitrary polarized optical waves in SALC transforms into the partially frequency degenerate FWM because each optical wave splits into the ordinary and extraordinary waves. The coupled optical waves create a dynamic grating of the smectic layer normal displacement $u(x, y, z, t)$ and undergo the parametric energy exchange and XPM. The signal optical waves with the lower frequency are amplified up to a saturation level determined by the Manley-Rowe relation, while the pumping optical waves with higher frequency are depleted. It has been shown that the system of the coupled optical waves and the dynamic grating is stable. The analytical expressions for the magnitudes and phases of SVA have been obtained in the limiting case when the waves are mainly polarized either perpendicular to the propagation plane, or in it. The SLS gain coefficient is significantly larger than the one in the case of the Brillouin SLS in isotropic organic liquids. The SLS in SALC also results in the generation of the Stokes and anti-Stokes harmonics with the combination wave vectors.

The nondegenerate FWM in SALC results in the amplification of the signal optical wave with the lowest frequency and depletion of three other waves with higher frequencies. The polarization-decoupled FWM may take place when the polarizations of some optical waves are perpendicular to one another. If the coupled optical waves are counter propagating and their frequencies satisfy the balance conditions typical for OPC process then BEFWM takes place accompanied by the amplification of the phase-conjugate wave. The spectrum of the scattered harmonics consists of 24 Stokes and anti-Stokes terms with combination frequencies and wave vectors.

LC applications in nanophotonics, plasmonics, and metamaterials attracted a wide interest due to the combination of LC large nonlinearity and strong localized electric fields of SPP. Until now, NLC applications in nanophotonics and plasmonics have been investigated. We studied theoretically the nonlinear optical processes at the interface of a metal and a homeotropically oriented SALC. In such a case, SPP penetrating into SALC create the spatially localized surface dynamic grating of smectic layer normal displacement. We have shown that for optical frequencies of about 10^{15} s^{-1} and coupled SPP frequency difference of about 10^{8} s^{-1}, the SALC-metal system cubic susceptibility may be one to two orders of magnitude larger than the cubic susceptibility of isotropic organic liquids. We solved the wave Eq. (13) for the counter-propagating SPP in SALC with the spatially localized nonlinear polarization and obtained the explicit expressions (55)–(57) for the magnitudes and phases of the coupled SPP SVA. It has been shown that the Rayleigh stimulated scattering of SPP on the surface smectic layer oscillations occurs. The rise time of the amplified SPP of about 10 ns can be achieved, which is much faster than the Brillouin relaxation constant in NLC.

The plasmonic waveguides with NLC for nanophotonic and plasmonic have been theoretically investigated. We proposed an MIM waveguide with an SALC core. We evaluated the electric field of the strongly localized SPP even mode, the smectic layer normal strain and the nonlinear polarization in the MIM core. The evaluation of the SPP SVA shows that the strong SPM process takes place. The SPM is enhanced by the geometric factor caused by the strong SPP localization in the MIM core.

Author details

Boris I. Lembrikov*, David Ianetz and Yossef Ben Ezra

*Address all correspondence to: borisle@hit.ac.il

Department of Electrical Engineering and Electronics, Holon Institute of Technology (HIT), Holon, Israel

References

[1] De Gennes PG, Prost J. The Physics of Liquid Crystals. 2nd ed. New York, USA: Oxford Univeristy Press; 1993. 597 p. DOI: ISBN: 978-0198517856

[2] Khoo I-C. Liquid Crystals. 2nd ed. Hoboken, New Jersey, USA: Wiley; 2007. 368 p. DOI: ISBN: 978-0-471-75153-3

[3] Khoo IC. Nonlinear optics of liquid crystalline materials. Physics Reports. 2009;**471**:221-267. DOI: 10.1016/j.physrep.2009.01.001

[4] Khoo IC. Nonlinear optics, active plasmonics and metamaterials with liquid crystals. Progress in Quantum Electronics. 2014;**38**(2):77-117. DOI: 10.1016/j.pquantelec.2014.03.001

[5] Kventsel GF, Lembrikov BI. Two-wave mixing on the cubic non-linearity in the smectic A liquid crystals. Liquid Crystals. 1994;**16**(1):159-172. DOI: ISSN: 0267-8292

[6] Kventsel GF, Lembrikov BI. Stimulated light scattering in smectic A liquid crystals. Liquid Crystals. 1995;**19**(1):21-37. DOI: ISSN: 0267-8292

[7] Kventsel GF, Lembrikov BI. Self-focusing and self-trapping in smectic A liquid crystals. Molecular Crystals and Liquid Crystals. 1995;**262**(1):629-643. DOI: ISSN: 1542-1406

[8] Kventsel GF, Lembrikov BI. The four-wave mixing and the hydrodynamic excitations in smectic A liquid crystals. Molecular Crystals and Liquid Crystals. 1995;**262**(1):591-627. DOI: ISSN: 1542-1406

[9] Kventsel GF, Lembrikov BI. Second sound and nonlinear optical phenomena in smectic A liquid crystals. Molecular Crystals and Liquid Crystals. 1996;**282**(1):145-189. DOI: ISSN: 1542-1406

[10] Lembrikov BI. Light interaction with smectic A liquid crystals: nonlinear effects. HAIT Journal of Science and Engineering. 2004;**1**(2):306-347. DOI: ISSN: 1565-4990

[11] Lembrikov BI, Ben-Ezra Y. Surface plasmon polariton (SPP) interactions at the interface of a metal and smectic liquid crystal. In: 17th International Conference on Transparent Optical Networks (ICTON 2015); July 5–9, 2015; Budapest, Hungary. 2015. p. We.C4.4, 1-4. DOI: 978–1–4673-7879-6/15

[12] Lembrikov BI, Ben-Ezra Y, Ianetz D. Stimulated scattering of surface plasmon polaritons (SPPs) in smectic A liquid crystal. In: 18th International Conference on Transparent Optical Networks (ICTON-2016); July 10–14, 2016; Trento, Italy. 2016. p. We.B4.2, 1-4. DOI: 978–1–5090-1466-8/16

[13] Lembrikov BI, Ianetz D, Ben-Ezra Y. Metal/Insulator/Metal (MIM) plasmonic waveguide containing a smectic A liquid crystal (SALC) layer. In: 19th International Conference on Transparent Optical Networks (ICTON 2017); July 2–6, 2017; Girona, Catalonia, Spain. 2017. p. Tu.A4.3, 1-4. DOI: 978–1–5386-0858-6/17

[14] Shen YR. The Principles of Nonlinear Optics. Hoboken, New Jersey, USA: Wiley; 2003. 563 p. DOI: ISBN: 0-471-43080-3

[15] Liao Y, Clark NA, Pershan PS. Brillouin scattering from smectic liquid crystals. Physical Review Letters. 1973;**30**(14):639-641. DOI: 10.1103/PhysRevLett.30.639

[16] Ricard L, Prost J."Second sound" propagation and the smectic response function. Journal DE Physique Colloque C3. 1979;**40**(supplement au no. 4):C3–83-C3–86. DOI: 10.1051/jphyscol:1979318

[17] Ricard L, Prost J. Critical behaviour of second sound near the smectic a nematic phase transtion. Journal De Physique. 1981;**42**(6):861-873. DOI: 10.1051//jphys:01981004206086100

[18] Vagner ID, Lembrikov BI, Wyder P. Electrodynamics of Magnetoactive media. 1st ed. Heidelberg, Germany: Springer; 2004. 422 p. DOI: ISBN: 3-540-43694-4

[19] Newell AC. Solitons in Mathematics and Physics. 1st ed. Philadelphia, PA, USA: Society for Industrial and Applied Mathematics; 1985. 244 p. DOI: ISBN: 978-08-9871-1967

[20] Khoo I-C, Michael RR, Yan P-Y. Simultaneous occurence of phase conjugation and pulse shortening in stimulated scattering in liquid crystal mesophases. IEEE Journal of Quantum Electronics. 1987;**23**(8):1344-1347. DOI: 10.1109/JQE.1987.10734497

[21] Svetlana G. Lukishova. Liquid crystals under two extremes: (1) high-power irradiation, (2) single-photon level. Molecular Crystals and Liquid Crystals. 2012;**559**:127-157. DOI: 10.1080/154221406.2012.658703

[22] Guang S. He. Optical phase conjugation: principles, techniques, and applications. Progress in Quantum Electronics. 2002;**26**(3):131-191. DOI: ISSN: 0079-6727

[23] Oliveri G, Werner DH, Massa A. Reconfigurable electromagnetics through metamaterials -a review. Proceedings of the IEEE. 2015;**103**(7):1034-1056. DOI: 10.1109/JPROC.2015.2394292

[24] Maier SA. Plasmonics: Fundamentals and Applications. 1st ed. New York, USA: Springer Science; 2007. 223 p. DOI: ISBN: 978-0387-33150-8

[25] Sarid D, Challener WA. Modern Introduction to Surface Plasmons. 1st ed. New York, USA: Cambridge University Press; 2010. 371 p. DOI: ISBN 978-0-521-76717-0

[26] Fedorov DO, Romanov VP, Ul'yanov SV. Surface oscillations of smectic-A liquid crystals. Physical Review E. 2000;**62**(1):681-688. DOI: 1063-651X/2000/62(1)/681(8)

[27] Robert W. Boyd. Nonlinear Optics. 3rd ed. Amsterdam: Elsevier; 2008. 613 p. DOI: ISBN: 978-0-12-369470-6

[28] Beeckman J, James R, Fernandes FA, De Cort W, Vanbrabant PJM, Neyts K. Calculation of fully anisotropic liquid crystal waveguide modes. Journal of Lightwave Technology. 2009;**27**(17):3812-3819. DOI: 10.1109/JLT.2009.2016673

[29] Zografopoulos DC, Becceherelli R, Tasolamprou AC, Kriezis EE. Liquid-crystal tunable for integrated plasmonic components. Photonics and Nanostructures - Fundamentals and Applications. 2013;**11**:73-84. DOI: 10.1016/j.photonics.2012.08.004

[30] Zografopoulos DC, Beccherelli R. Liquid-crystal-tunable metal-insulator-plasmonic waveguides and Bragg resonators. Journal of Optics. 2013;**15**:1-5. DOI: 10.1088/2040-8978/15/5/055009

[31] Prokopidis KP, Zografopoulos DC, Kriezis EE. Rigorous broadband investigation of liquid-crystal plasmonic structures using finite-difference time-domain dispersive-anisotropic models. Journal of Optical Society of America B. 2013;**30**(10):2722-2730. DOI: 10.1364/JOSAB.30.002722

IntechOpen